Bulk composites from microfibrillated cellulose made into a superior mechanical–performance structural material through lignocellulose/borate cross–linking

Huajie Shen (shenghuajie@fjut.edu.cn)
Fujian University of Technology
Liangzhou Dong
Fujian University of Technology
Xinyuan Zheng
Fujian University of Technology
Yifan Jiang
Fujian University of Technology

Article

Keywords:

Posted Date: December 12th, 2022

DOI: https://doi.org/10.21203/rs.3.rs-2348579/v1

Additional Declarations: No competing interests reported.

BULK COMPOSITES FROM MICROFIBRILLATED CELLULOSE MADE INTO A SUPERIOR MECHANICAL–PERFORMANCE STRUCTURAL MATERIAL THROUGH LIGNOCELLULOSE/BORATE CROSS–LINKING

Correspondence and requests for materials should be addressed to: Huajie Shen (shenghuajie@fjut.edu.cn)

Title: Bulk composites from microfibrillated cellulose made into a superior mechanical–performance structural material through lignocellulose/borate cross–linking

Author names: Huajie Shen[1, 2, *], Liangzhou Dong[1], Xinyuan Zheng[1], Yifan Jiang[1]

Affiliations: 1. School of Design, Fujian University of Technology, Fuzhou 350118, Fujian, People's Republic of China; 2. Research and Development Department of Huzhou Boloni Technology Co., Ltd, Huzhou, Zhejiang 313029, People's Republic of China.

Abstract: Since the cross-linking of borates strengthens the structural connection between cells, mechanically superior structural material based on lignocellulose/borate is synthesized using a s mechanical pretreatment method and a binder free hot-pressing method. The results show that the pine lignocellulose formed a dense laminated structure after compressive force, shears, and friction forces and hot–pressing. And microfibrillated cellulose material retained the chemical composition of untreated lignocellulose and the mechanical milling processes of active hydroxyl groups formed by the condensation reaction of borate orthoester with furfural resin adhesive. The flexural strength, modulus elasticity and internal bonding strength of microfibrillated cellulose material are 5, 2.5 and 4.1higher than the untreated lignocellulose specimen, respectively. Furthermore, the thickness swelling rate was 5.66%, which are 298% lower than untreated lignocellulose specimen, indicating its excellent dimensional stability. This is mainly due to the layering and branching of pine lignocellulose during mechanical milling, which gives it more ester and hydrogen bonds, expanding the ratio to surface area and exposing more hydroxyl groups. And the formation of furfuryl alcohol occurred in the hot-pressing process, including the degradation of monosaccharides to furfural, the condensation reaction between lignin and furfural, the resinization of furfural, and the formation of hydrogen bonds. The resulting stable laminated covalent cross–linking structure and the cross–linking of nano–lignocellulose/borate ensure that the material has an excellent mechanical performance, which provides some unique strategies and theoretical guidance to design a superior mechanical–performance structural material from lignocellulose.

Introduction

Wood is one of complex organisms [1]. It relies on a microscopically strong cell wall to develop into self-sustaining macroscopic organisms [2]. And the cell wall consists primarily of microscopically large numbers of tiny cells of the lignin, cellulose, and

hemicellulose [3, 4], each with a precise structure, including tiny openings, membranes, and intricate laminar walls [1]. Among them, lignin is what holds cellulose and hemicellulose cells together, while boronate connections are what form the reinforced intercellular network [5, 6]. The wood contains very low concentrations of the boric acid cross-linked polysaccharide rhamnogalacturonan II [7, 8], enhancing the cell wall [7]. It provides wood with the support strength to improve the material performance of the intercellular structure and the material surrounding its individual cell walls, allowing it to resist gravity and strong lateral force [9, 10]. Because boric acid ion can form strong covalent bonds with oxygen-containing functional groups, which is an excellent cross-linker for higher plants [11, 12]. Inspired by the cross-linking of borates in plants, self-bonding cross-linking between borates and graphene nanosheets has been studied [13, 14], which has an important effect in enhancing the strength and survival functions of plants [15, 16]. In addition, it is low-toxic, highly active, non-flammable and non-corrosive, while also exhibiting antibacterial and antifungal properties [17], and thus has been shown to be effective in the binderless lignocellulose composites have potential applications in the field.

Microfibrillated cellulose are widely used and there is an inexhaustible high-performance nanolignocellulose in wood [18, 19]. And the main sources of lignocellulose are agricultural waste, forestry waste, processing residues and domestic waste [14, 20, 21]. Mainly includes crop residues and crop livestock [22]; forestry waste mainly includes forestry "three residues" and waste woody materials [23]; processing waste mainly includes agricultural processing waste and industrial processing waste [24]; domestic waste mainly includes urban domestic waste resources [25]. Due to its abundance of sustainable substances starting from the use of waste resources, it is gaining attention as an alternative to synthetic materials, so that waste resources become the main body of biomass resources [21, 26]. The development and utilization of lignocellulose-based materials can alleviate resource stress, release environmental pressure, improve living standards and economic growth [19]. Maintaining ecological balance; developing biomass energy and utilizing waste resources, not only solving the problem of environmental pollution, but also solving the problem of renewable energy from raw materials [27]. Sustainability issues provide the basis for strategic research on the development of renewable energy to achieve fast and good sustainable development.

Here, to overcome the problem of insufficient adhesion of microfibrillated cellulose binderless laminates, the cross–linking between borate ions and polysaccharide rhamnogalacturonan II molecules was utilized, inspired by higher plants. A mechanical pretreatment method and binderless hot–press method was developed to prepare superior mechanical–performance structural material based on lignocellulose/borate cross–linking. Use of furfuryl alcohol formation, including degradation of monosaccharides to furfural, condensation reactions of lignin and furfural, resinization of furfural, and hydrogen bond formation, which can increase the crosslinking of the microfibrillated cellulose material and ensure the toughness of stable laminar covalent cross–linking structure after binderless hot–pressing. The as–prepared microfibrillated cellulose material exhibited excellent mechanical performance, which is due to the enhancement effect caused by format borate, and borate–diol ester, ensuring that the adhesive possessed bond strength.

Results and discussion

The preparation process of microfibrillated cellulose material by binderless hot pressing is shown in **Fig. 1**, Including swelling, colloid milling, and binderless hot–pressing. The nanolignocellulose/borate cross–linked network is formed between two polysaccharides.

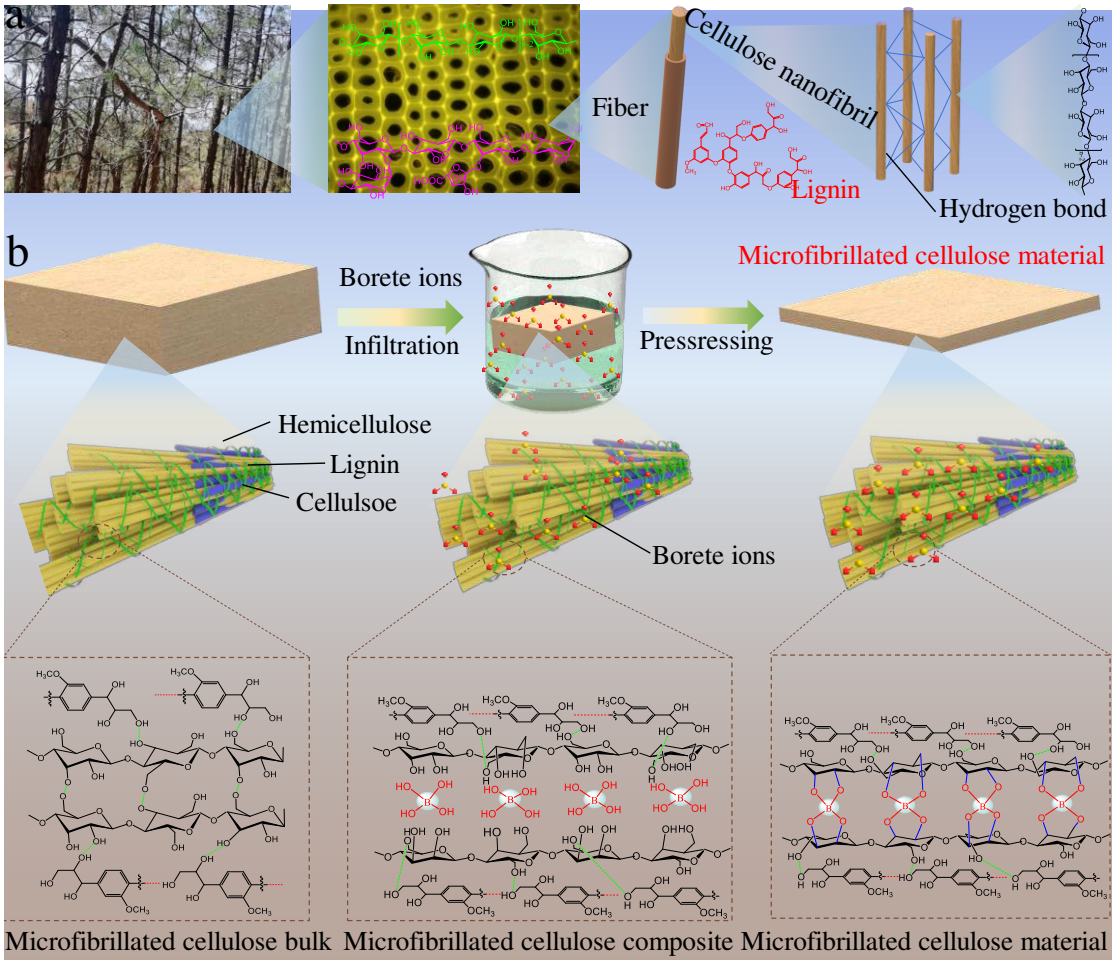

Fig. 1 Illustration of the synthesis of microfibrillated cellulose material. a, Digital picture of *Pinus Yunnanensis* Franch, Electron microscopy image of a 10 μm thick cross section of *Pinus Yunnanensis* Franch. Schematic illustration of the cellulose nanofibrils pulping of wood blocks that degrade the lignin rapidly. b, schematic of stable covalent crosslinking structure and nanolignocellulose/borate cross–linking interconnected cell wall in Pine lignocellulose.

The micro–morphology of the untreated lignocellulose is shown in **Fig. 2a**. The untreated lignocellulose was slender and smooth, and the pits are clearly visible at high magnification (**Fig. 2a** inset). The cross–section macroscopic and microscopic–morphology of untreated lignocellulose specimen are shown in **Fig. 2b**. The pine-lignocellulose interlaces in a long, thin, and disorderly manner. **Fig. 2c** displays micro–morphology of microfibrillated cellulose by mechanical hot rubber milling, which a clear stratification can be observed. At high magnification (**Fig. 2c insert**), microfibrillated cellulose was effectively combined. This may be that boric acid forms a covalent bond with polysaccharide by hot–pressing, so that the microfibrillated cellulose molecular chains are crosslinked. The compressive force, shears and friction forces generated by the mechanical milling processes of untreated

lignocellulose with a colloid mill result in a laminar structure of pine lignocellulose. **Fig. 2d** shows the cross–section macroscopic and microscopic–morphology of the microfibrillated cellulose material, which obviously dense stratification structure could be observed.

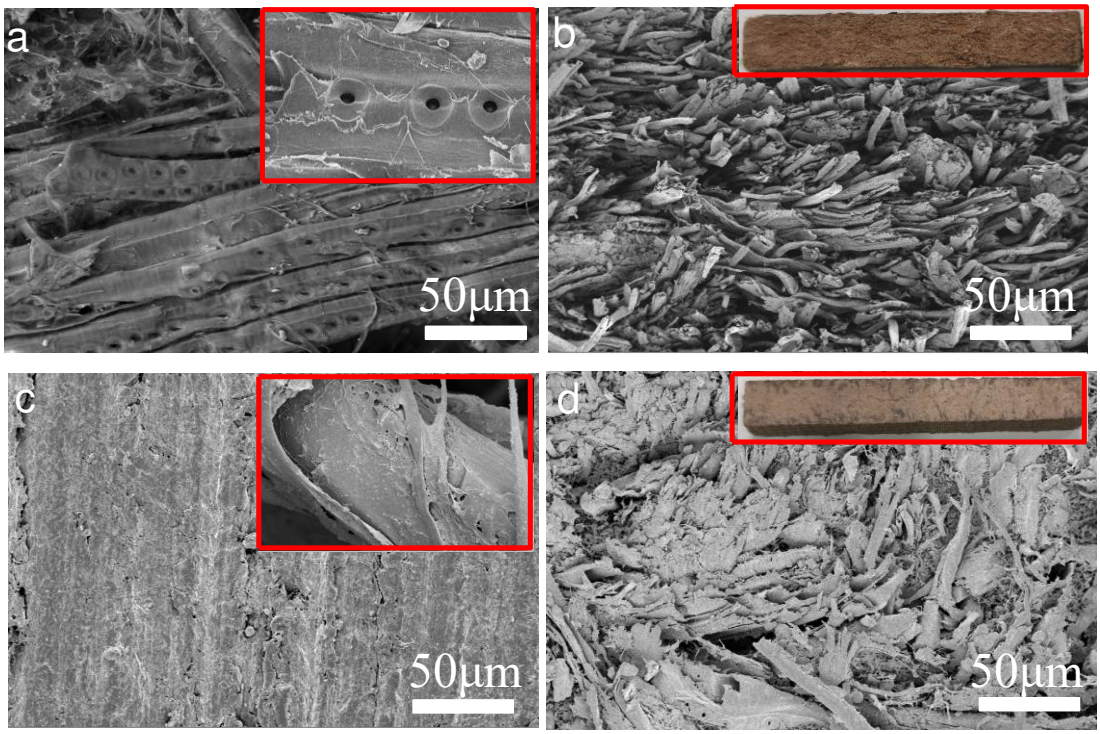

Fig. 2 (a) SEM of pine lignocellulose, (b) SEM of the cross section of untreated lignocellulose, (c) SEM of microfibrillated cellulose, (d) SEM image of the cross section of microfibrillated cellulose material.

The XRD spectrum of the untreated lignocellulose specimen and microfibrillated cellulose material are displayed in **Fig. 3a-c**, there are no distinctive characteristic peak could be observed except those of the characteristic peaks of cellulose at 16 and 22 degrees, which are characteristic peaks of the typical reflective surfaces (110) and (002) of pine lignocellulose. And the microfibrillated cellulose material, there is no obvious change between the XRD spectrum of the characteristic peaks of untreated lignocellulose specimen and microfibrillated cellulose material, but its relative crystallinity increases. Compared with the XRD peaks of the untreated lignocellulose specimen, except for relative crystallinity increases of the characteristic peaks, the XRD peaks here are in consistent of the relative crystallinity increases peaks. The results show that the microfibrillated cellulose material has high phase purity, consisting only of the products of the pine nanolignocellulose as well as the products after hydroxymethylation.

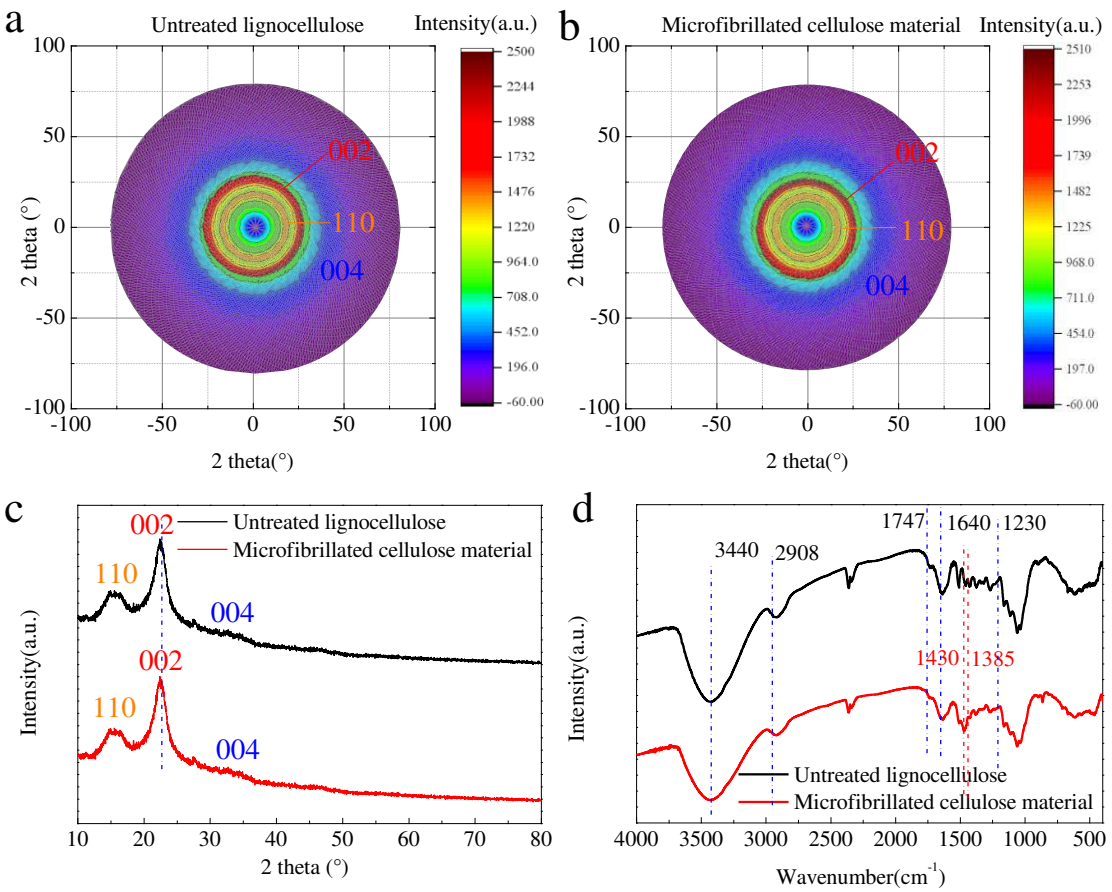

Fig. 3 (a-c) XRD patterns of untreated lignocellulose and microfibrillated cellulose material. (b) FTIR patterns of untreated lignocellulose and microfibrillated cellulose material, respectively.

FTIT spectra of untreated lignocellulose specimen and microfibrillated cellulose material are shown in **Fig. 3d**. The FTIR spectra of the microfibrillated cellulose material had little change compared with that of the untreated lignocellulose specimen, but the absorption bands of microfibrillated cellulose material at 1100–1230 cm^{-1}, 1700–1725 cm^{-1} and 3650–3200 cm^{-1} have changed significantly. The FTIT spectra of the microfibrillated cellulose material was similar to the rubber milled lignocellulose, indicating that the chemical structure of lignocellulose after mechanical and thermal rubber milling is not destroyed in microfibrillated cellulose material, and characteristics of lignocellulose maintained well. Comparing the FTIT spectra of t untreated lignocellulose specimen and microfibrillated cellulose material, the broad peak at 3440 cm^{-1} corresponds to the –OH, indicating that the –OH occurs during rubber milling; the C–H stretching vibration peak at 2908 cm^{-1} is characteristic peak of cellulose. The peak at 1430 cm^{-1} is the bending vibration of CH_2 in lignin and polysaccharides. The peak at 1385 cm^{-1} corresponds to the bending vibration of C–H in cellulose and hemicellulose. The peak at 1747 cm^{-1} The C=C characteristic peak of the aromatic ring stretches and vibrates, indicating the presence of lignin. The enhancement of the absorption peak at 1230 cm^{-1} is due to the lignin is a phenolic substance formed during the mechanical rubber grinding process. The results show that the microfibrillated cellulose material retained the chemical composition and active hydroxyl groups formed by condensation reaction of borate orthoester

formation and furfural resin adhesive. The analytical results correspond to the reaction mechanism in the **Fig. 1**, below: Formation of hydrogen bonds and covalent bonds.

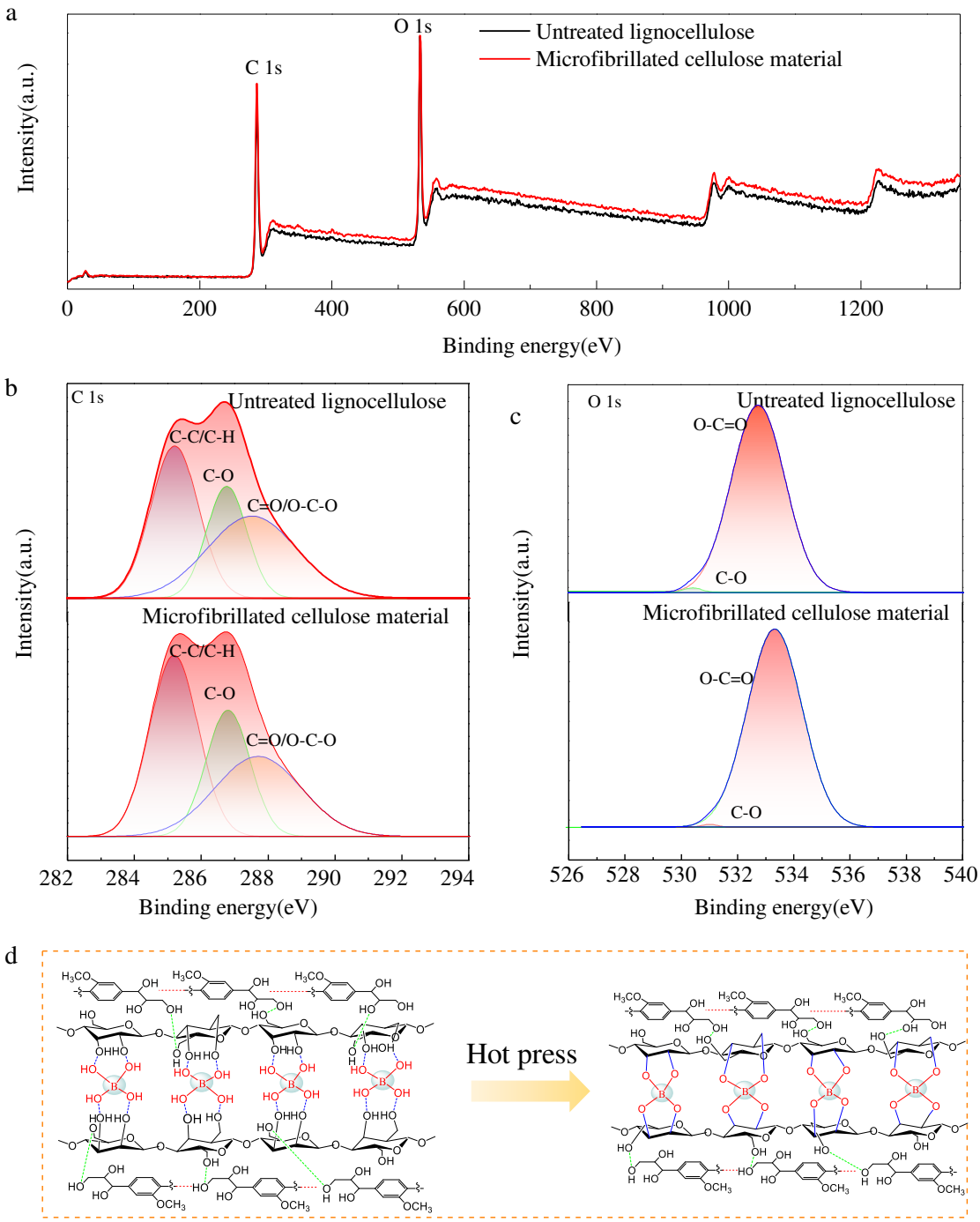

Fig. 4 Survey XPS untreated lignocellulose specimen and microfibrillated cellulose material (a); C 1s(b) and O 1s (c) of untreated lignocellulose specimen and microfibrillated cellulose material, respectively. d, Schematic illustration of the formation of the borate crosslinked network.

The XPS spectrogram of untreated lignocellulose specimen and microfibrillated cellulose material are shown in **Fig.4**. The survey spectrum of samples is shown in **Fig. 4a**. For comparison, the main chemical composition of the pre–treated wood

surface remained unchanged and consisted mainly of C, H and O elements in the energy of 285.69 eV and 532.67 eV. Fig. 4b Spectral peaks of C1s for the untreated lignocellulose specimen and microfibrillated cellulose material, respectively. The three small peaks under the outer contour were obtained by the peak decomposition technique, and the outer contour largely overlaps with the synthetic curves of the three small peaks, indicating that the fitting The absence of C4 in the peak of the C 1s spectrum may be due to the fact that the sample was colloid to contain very few carboxylic acid groups, while the relatively low resolution of the surface photoelectron spectrometer used is also one of the reasons. The three small peaks represent carbon atoms in different chemical structures, namely C1, C2 and C3. After milling, the C–C bond content decreased significantly, while the C3 content increased significantly, indicating that a large number of oxygen–containing functional groups were produced on the wood surface. The content of O2 in the untreated lignocellulose specimen is less and O1 content is more, indicating that the untreated lignocellulose specimen surface oxygen and carbon cross–linked mainly for the C–O single bond, and through the double bond is linked to carbon with less oxygen, while the O_2 content of the microfibrillated cellulose material is increased and the O1 content is decreased. At the same time, the C/O values of elements and the percentages of C and O in different chemical states are shown in **Table 1**. The O2/O1 is increased, which indicates an increase in the oxidation state of carbon in the pretreated wood. The increase of peak O2 is due to the oxidative condensation of lignin to produce many carbonyl groups. The decrease of O1 peak area is due to the dehydration of the cellulose and the degradation of hemicellulose resulting in the oxidation of the sample. Moreover, it can also be seen from the table that the milling pretreatment have the largest nO2/nO1, indicating that the untreated lignocellulose specimen produces C=O content highest. The XPS spectra shown that boric acid formed covalent bond with the –OH group of the polysaccharide. The resulting stable covalent crosslinking structure and nanolignocellulose/borate cross–linking guarantee outstanding bond strength, as shown in **Fig. 4d**. The resulting stable covalent crosslinked structure with synergistic hydrogen bonding ensures that the adhesive of microfibrillated cellulose exhibits dramatic bond strength and water tolerance.

Table 1 Element content and O/C ratios of untreated lignocellulose specimen and microfibrillated cellulose material

Specimen	**Peak position(eV)**			**Peak area (%)**		
	C1	C2	C3	C1	C2	C3
Untreated lignocellulose specimen	285.21	286.76	287.52	37.98	23.58	38.45
Microfibrillated cellulose material	285.18	286.80	287.69	35.32	26.08	38.60

Specimen	**Peak position(eV)**		**Peak area(%)**		**nO2/nO1**
	O1	O2	O1	O2	
Untreated lignocellulose specimen	533.25	531.27	99.91	0.09	0.0009
Microfibrillated cellulose material	533.31	531.01	99.62	0.38	0.0038

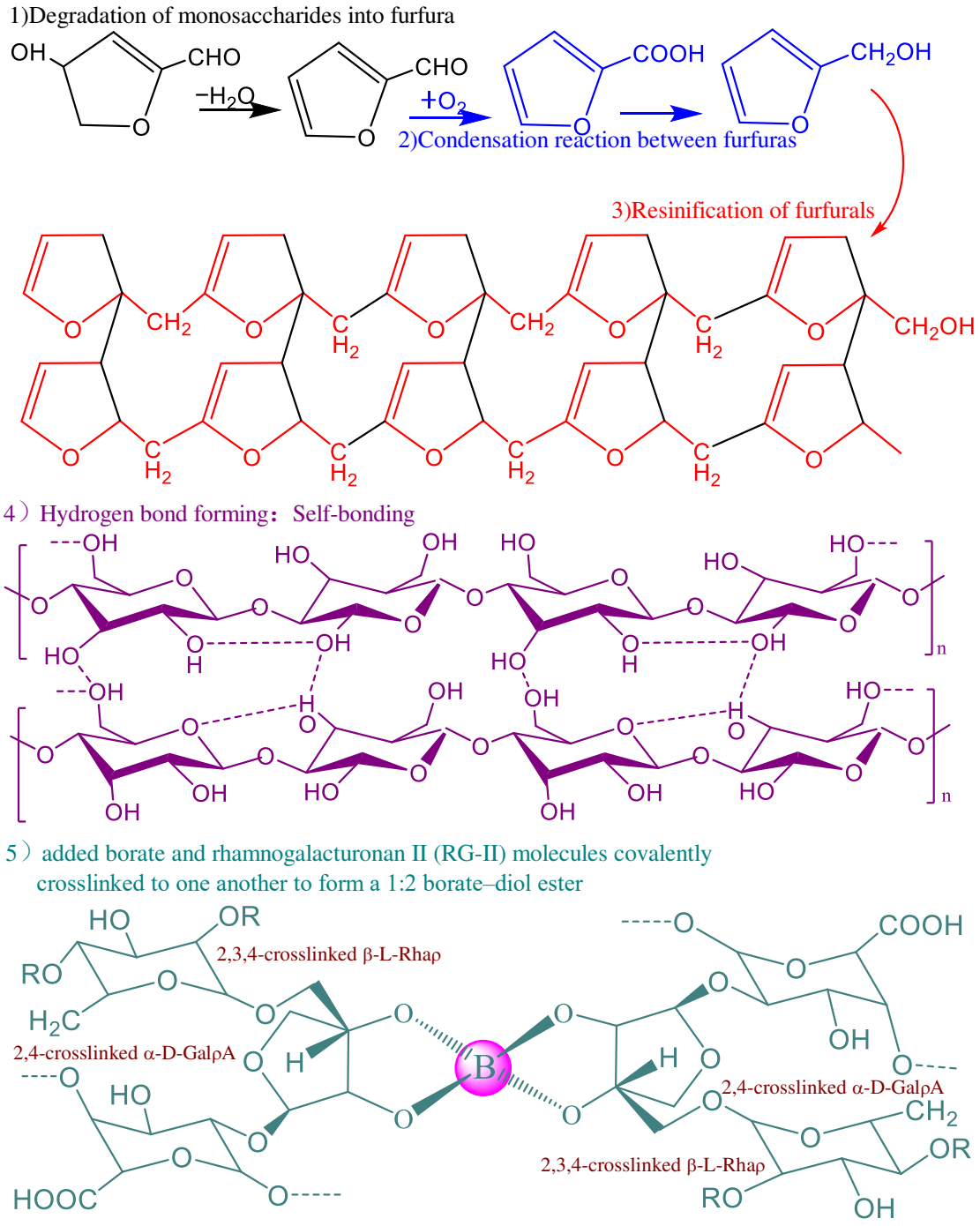

Fig. 5 Furfuryl alcohol formation processes.

The processes of furfuryl alcohol formation and condensation reaction and resinification, including 1) monosaccharides degradation to furfural, 2) condensation reactions between furfural, 3) furfural resinization, hydrogen bond formation process and borate and polysaccharide rhamnogalacturonan II molecules covalently crosslinked, as shown in **Fig. 5**. Binderless hot–pressing produces formic acid and acetic acid due to the degradation of microfibrillated cellulose, which promotes the densification of pine lignocellulose. This is because the low molecular weight monosaccharides of degraded pine lignocellulose can be further degraded to furfural. In addition to the above–mentioned binding modes, the resin between furfural cross-linked during hot-pressing process. Meanwhile, the oxygen atom on the

hydroxyl group in lignocellulose can be covalently cross-linked or hydrogen bonded to the hydrogen atom on the same hydroxyl group. As the moisture in the plate embryo evaporates by hot pressing, the surface tension brings the cellulose close to each other and covalently bonds. Meanwhile, boracic acid in the microfibrillated cellulose effectively forms covalent bonds with the cellulose and hemicellulose in the degradation of microfibrillated cellulose by hot-pressing, forming –OH groups of polysaccharides such as glucose, xylose, glucomannan, arabinose and other monosaccharides, resulting in a stable covalent crosslinking structure. This non–adhesive microfibrillated cellulose material is guaranteed to exhibit excellent bond strength due to the stable borate and polysaccharide rhamnogalacturonan II molecules covalently crosslinked structure.

Fig. 6a shows the flexural strength and modulus of untreated lignocellulose specimen and microfibrillated cellulose material, which are 80.27 N and 6498MPa that are 5 and 2.5 times as much as the untreated lignocellulose specimen, and 2.5 and 2.7 times as much as the Chinese national standard No. GB/T11718–2009, respectively. This is due to the enhancement caused by the formation of furfuryl alcohol and borate-diol ester. The stress–displacement curves of three kinds of untreated lignocellulose specimen and microfibrillated cellulose material are shown in **Fig.6b**. Average maximum loads of two specimens are 21.44N and 115.27N, respectively. The flexural strength of microfibrillated cellulose material is the highest. The mechanical performance of microfibrillated cellulose material is better than those of untreated lignocellulose specimen and relevant indicators of standard GB/T11718–2009. The IB value of microfibrillated cellulose material was 0.880 MPa, which was 4.1 times as much as the untreated lignocellulose specimen and 1.8 times as much as the relevant indicators of standard GB/T11718–2009 (**Fig.6d**), while TS was only 5.66%, which was 298% lower than that of untreated lignocellulose specimen (**Fig.6c**). This is mainly due to the layering and branching of pine lignocellulose during the mechanical milling processes, which gives it more ester and hydrogen bonds, enlarges the specific surface area, exposing more hydroxyl groups, and increases the cross–linking degree between borate and polysaccharide rhamnogalacturonan II molecules with a condensation reaction among furfurals, lignin, and furfurals during hot–pressing. The results indicated that excellent mechanical performance of microfibrillated cellulose material is superior to those of untreated lignocellulose specimen and relevant indicators of standard GB/T11718–2009 and other biomass materials.

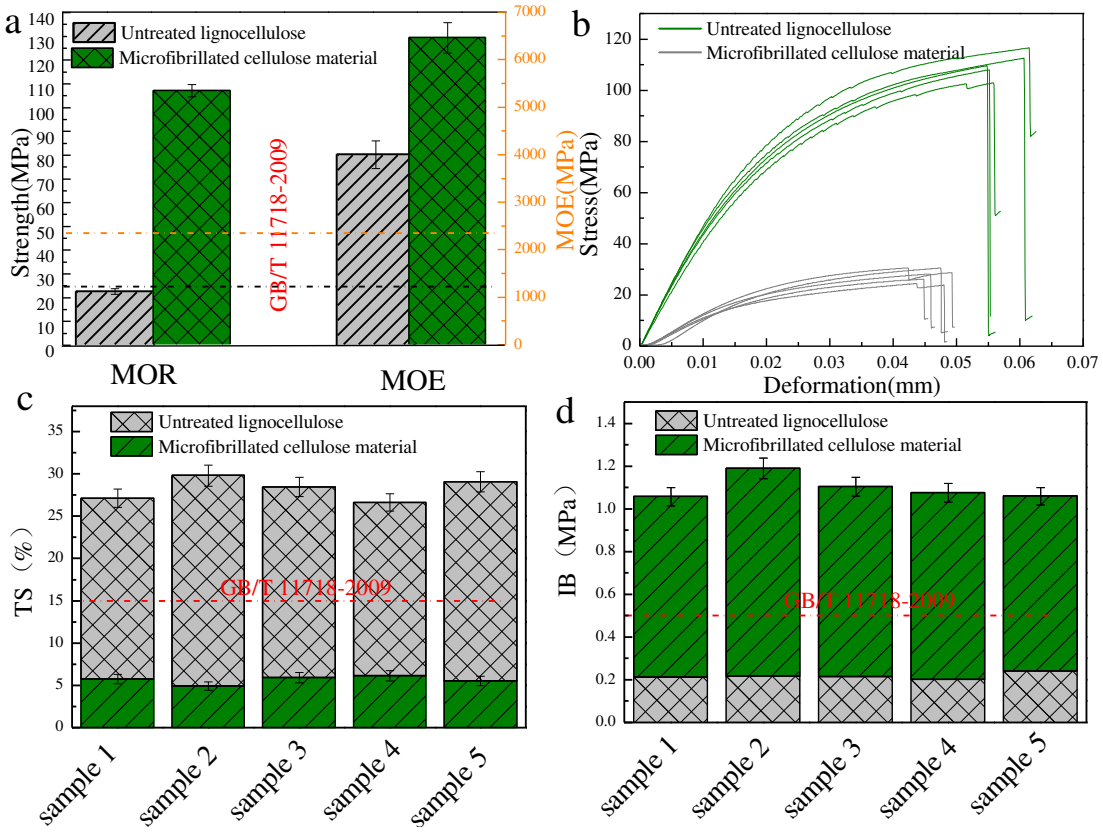

Fig. 6 The mechanical strength histogram (a), the stress–deformation curves(b), the TS (c) and the IB (d) of untreated lignocellulose specimen and microfibrillated cellulose material

The simplified structural schematics of quasi-static three-point bending test is shown in **Fig.7a**, showing the alternating arrangement of nanolignocellulose building blocks. And under the action of three-point bending, microfibrillated cellulose material began to slide and deflect cracks, activating the potential sliding of nanolignocellulose building blocks of microfibrillated cellulose material. Finally, microfibrillated cellulose material fails under the building blocks fracture mode of nanolignocellulose. Interestingly, in microfibrillar cellulose materials, the hydrogen bonding between nanolignocellulose building blocks and the laminated structure induced synergistic effect (**Fig. 7a**). **Fig. 7b** shows the mechanical properties of microfibrillated cellulose materials compared with those of lignocellulose matrix composites. Apparently, the microfibrillated cellulose materials thus present a combination of better ultimate flexural strength and elastic modulus that offers considerable advantage for high specific strength engineering material, such as lignocellulose-based composites, wood fiber-based composites, plexiglass, inorganic composite material, and nacre, show poor mechanical stabilities. It can be seen that the mechanical performance of microfibrillated cellulose materials is superior to many natural and wood fiber/lignocellulose-based composite materials.

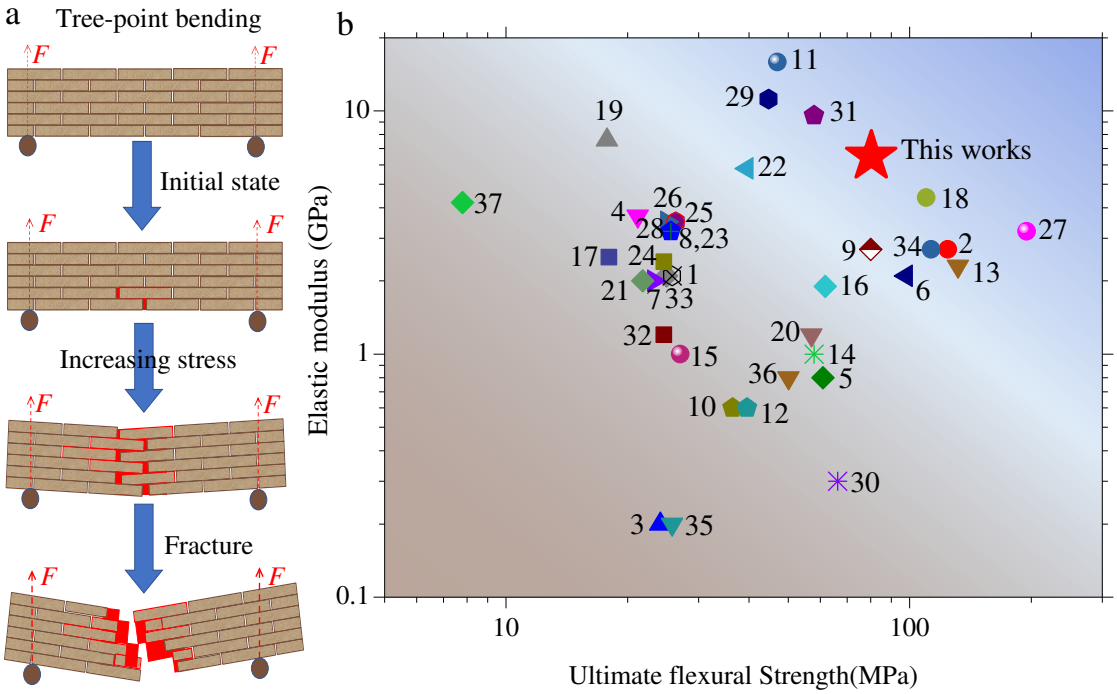

Fig. 7 (a) Proposed synergistic mechanism of microfibrillated cellulose material. (b) Ashby diagram of ultimate flexural strength and elastic modulus for the microfibrillated cellulose material and various natural and artificial composites.

Conclusions

Microfibrillated cellulose material with superior mechanical–performance was successfully developed by a mechanical pretreatment method and hot-pressing method. The result showed that the core layer of microfibrillated cellulose material has good compactness, which effectively enhances the flexural strength and elastic modulus of microfibrillated cellulose material. Compared with untreated lignocellulose, MOR, MOE, IB value increased by 5, 2.5 and 4.1times, TS value decreased by 298%. And excellent mechanical properties of microfibrillated cellulose material are superior to those of untreated lignocellulose specimen and relevant indicators of standard GB/T11718-2009 and other biomass materials. This is due to the enhancement caused by the formation of furfuryl alcohol and borate-diol ester. The nano-lignocellulose/borate cross-linking ensures bonding strength. With the development of borate cross–linking networks, lignocellulose–based superior mechanical–performance structural material can be applied in more fields, broaden the development space of lignocellulose–based superior mechanical–performance structural material industry, and at the same time, it is expected that microfibrillated–cellulose/nanolignocellulose will become an advanced structural–functional integrated new material.

Materials and Methods

Plant materials. Lignocellulose (*Pinus Yunnanensis* Franch, Water content: 15%) was purchased from Southwest Timber Market in *Kunming*, Yunnan Province, China. Sodium tetraborate decahydrate was purchased from Yunnan Husen Trading Co., Ltd.

Preparation of the Microfibrillated Cellulose Material

Dry lignocellulose was mixed with deionized water of the ratio of 39:1 (wt. 2.5%). After then, swelling for 1 hour at 60 ℃, then the pine lignocellulose was placed into a colloid grinder and the colloid mill with rotation speed set 2880 rpm for 6 hours. After grinding, homogeneous microfibrillated cellulose glue was processed to about 100% water content, and then the microfibrillated cellulose material was developed through the binderless hot–pressing for 30 minutes (hot pressing temperature 200 ℃, pressure 2.5 MPa, thickness 10mm).

Characterization

The micro–morphologies of untreated lignocellulose specimen and microfibrillated cellulose material were measured by scanning electron microscopy (SEM, Quanta 200, FEI) and the 10–20 μm thick section of Yunnan–pine were observed under a, in Nikon biological microscope image analyzer (CELIPSE 80i, Nikon, Japan), cutting with a Leica slicer (SM2000R, Leica, Buffalo Grove). The crystal structure of the untreated lignocellulose specimen and microfibrillated cellulose material were determined by X–ray diffraction spectroscopy (XRD, Rigaku, D8 Advance, Bruker): nickel–filtered copper *Ka*–ray (λ = 1.5418 Å), 2° min $^{-1}$, current 40 mA, voltage 40 kV, characterized 5° –60°. Chemical Groups on the Surface of the untreated lignocellulose specimen and microfibrillated cellulose material were detected by FT–IR (FTIR, Nicolet iN10 MX, USA) and XPS (XPS, Thermo ESCALAB 250XI, USA). The physical and mechanical properties of the untreated lignocellulose specimen and microfibrillated cellulose material were measured according to the GB11718–2009 by *Shenzhen New Sansi* 50kN universal mechanical testing machine.

Data Availability

Te datasets generated during the current study are available from the corresponding author on reasonable request.

Acknowledgements: This study was financially supported by Enterprise scientific research project of Huzhou Boloni Technology Co., Ltd (Granted No.:2021ZD01A).

Author Contributions: Huajie Shen conceived and designed the study. Liangzhou Dong performed the experiments and identified the plant samples. Xinyuan Zheng wrote the main manuscript text. Yifan Jiang prepared figures and analyzed the data. All authors read and approved the manuscript.

References

1 Shmulsky, R. & Jones, P. D. Composition and Structure of Wood Cells. (Wiley - Blackwell, 2011).

2 Flores, E. I. S., Murugan, M. S., Friswell, M. I. & Neto, E. A. D. S. Computational multi-scale constitutive model for wood cell wall and its application to the design of bio-inspired composites. Proceedings of SPIE - The International Society for Optical Engineering 7975 (2011).

3 Zhang, X., Chen, S. & Xu, F. Combining Raman Imaging and Multivariate Analysis to Visualize Lignin, Cellulose, and Hemicellulose in the Plant Cell Wall. Journal of Visualized Experiments (2017).

4 R.M., R. & W.D., E. in ACS symposium series American Chemical Society.

5 Huang et al. Hemicellulose Composition in Different Cell Wall Fractions

Obtained using a DMSO/LiCl Wood Solvent System and Enzyme Hydrolysis. Journal of Wood Chemistry & Technology (2016).
6 Terashima, N. et al. Nanostructural assembly of cellulose, hemicellulose, and lignin in the middle layer of secondary wall of ginkgo tracheid. Journal of Wood Science 55, 409-416 (2009).
7 Darvill, O. N. M. A. T. I. P. A. A. G. RHAMNOGALACTURONAN II: Structure and Function of a Borate Cross-Linked Cell Wall Pectic Polysaccharide. Annual Review of Plant Biology 55, 109-139 (2004).
8 Ryden, P., Sugimoto-Shirasu, K., Smith, A. C., Findlay, K. & Mccann, R. M. C. Tensile Properties of Arabidopsis Cell Walls Depend on Both a Xyloglucan Cross-Linked Microfibrillar Network and Rhamnogalacturonan II-Borate Complexes. Plant Physiology 132, 1033-1040 (2003).
9 Burton et al. Heterogeneity in the chemistry, structure and function of plant cell walls. Nature Chemical Biology (2010).
10 Davison, B. H., Davis, M. F., Parks, J. M. & Donohoe, B. Plant Cell Walls: Basics of Structure, Chemistry, Accessibility and the Influence on Conversion - Aqueous Pretreatment of Plant Biomass for Biological and Chemical Conversion to Fuels and Chemicals. (2008).
11 Kinnaert, C., Daugaard, M., Nami, F. & Clausen, M. H. Chemical Synthesis of Oligosaccharides Related to the Cell Walls of Plants and Algae. Chemical Reviews, acs.chemrev.7b00162 (2017).
12 M A, O. N. S., Eberhard ; P, Albersheim ; A G, Darvill. Requirement of Borate Cross-Linking of Cell Wall Rhamnogalacturonan II for Arabidopsis Growth. Science 294, 846-849 (2001).
13 Soyekwo, F. et al. Borate crosslinking of polydopamine grafted carbon nanotubes membranes for protein separation. Chemical Engineering Journal 337, 110-121 (2018).
14 Chen, Y. et al. Bio-inspired layered nanolignocellulose/graphene-oxide composite with high mechanical strength due to borate cross-linking. Industrial Crops and Products 118, 65-72 (2018).
15 Wang, Z. & Pan, Q. An Omni‐Healable Supercapacitor Integrated in Dynamically Cross‐Linked Polymer Networks. Advanced Functional Materials 27, 1700690 (2017).
16 An, Z., Compton, O. C., Putz, K. W., Brinson, L. C. & Nguyen, S. B. T. Bio-Inspired Borate Cross-Linking in Ultra-Stiff Graphene Oxide Thin Films. Advanced Materials 23, 0-0 (2011).
17 Ottomeyer, M., Mohammadkah, A., Day, D. & Westenberg, D. Broad-Spectrum Antibacterial Characteristics of Four Novel Borate-Based Bioactive Glasses. Advances in Microbiology 06, 776-787 (2016).
18 Mussana, H. et al. Preparation of lignocellulose aerogels from cotton stalks in the ionic liquid-based co-solvent system. Industrial Crops & Products 113, 225-233 (2018).
19 Deepa, B. et al. Utilization of various lignocellulosic biomass for the production of nanocellulose: a comparative study. Cellulose 22, 1075-1090 (2015).

20 Stolarski, M. J., Krzyżaniak, M., Łuczyński, M., Załuski, D., Szczukowski, S., Tworkowski, J., Gołaszewski, J., . Lignocellulosic biomass from short rotation woody crops as a feedstock for second-generation bioethanol production. Industrial Crops & Products 75, S0926669015300285 (2015).

21 Cheng, Q., Duan, J., Zhang, Q. & Jiang, L. Learning from nature: constructing integrated graphene-based artificial nacre. Acs Nano 9, 2231 (2015).

22 Islam, M. S. Utilization of Crop Residues and Crop-Livestock Interaction in Rural Household in Bangladesh. (2013).

23 Chen, C. Advances in Research on the Preparation of Activated Carbon from Agricultural and Forestry Waste Material by Microwave Irradiation. Materials Review 3, 181-211 (2007).

24 Buyantuev, S. L., Ning, G., Kondratenko, A. S., Ye, J. & Guo, S. Waste Industrial Processing of Boron-Treated by Plasma Arc to Produce the Melt and Fiber Materials. (Springer Singapore).

25 Lima, J. S., Queiroz, J. E. G. D. & Freitas, H. B. Effect of selected and non-selected urban waste compost on the initial growth of corn. Resources Conservation & Recycling 42, 309-315 (2004).

26 Zhang, L. et al. Preparation of High-Strength Sustainable Lignocellulose Gels and Their Applications for Antiultraviolet Weathering and Dye Removal. ACS Sustainable Chemistry & Engineering (2019).

27 Aihara, Y. & Asano, Y. THE LUMBER PRODUCTION FOR BUILDINGS WHICH PRESUPPOSED MAINTAINING CO_2 BALANCE IN THE FOREST AND UTILIZING OF WOODEN BIOMASS ENERGY : Study on the utilization of wooden biomass in lumber production for buildings based on the premise of resources recycling. Journal of Environmental Engineering 72, 33-39 (2007).

Supplementary Files

This is a list of supplementary files associated with this preprint. Click to download.

- 20220110Manuscriptsp.pdf